Modelling of transport, adsorption and surface reaction kinetics on Ni, Pd and Ru metallic/acidic catalyst sites during hydrodeoxygenation of furfural

Rok Šivec, Brett Pomeroy, Matej Huš, Blaž Likozar, Miha Grilc *

Department of Catalysis and Chemical Reaction Engineering, National Institute of Chemistry, Ljubljana 1001, Slovenia

ARTICLE INFO

ABSTRACT

The furfural hydro-treatment process over Ni/Al$_2$O$_3$, Ni/SiO$_2$, Pd/Al$_2$O$_3$, Pd/SiO$_2$, Ru/Al$_2$O$_3$ and Ru/SiO$_2$ was investigated in a three-phase batch reactor operation at 150 °C, 175 °C and 200 °C, 60 barg hydrogen and tetrahydrofuran as solvent. The strength and rate of adsorption and desorption to/from acidic, metallic and interface site structures were determined, using H$_2$ temperature-programmed reduction (H$_2$-TPR), CO (CO-TPD) and NH$_3$ (NH$_3$-TPD) desorption experiments, and subsequent regression analysis of the results by numerical modelling and optimisation. To quantify the contribution of transport, active metal materials and support effect relationship, a generalized micro-kinetic model was postulated, which has been shown to describe experimental result outcomes well. Mechanistic description and regression analysis were applied to evaluate the role of the support (Al$_2$O$_3$ or SiO$_2$) on the catalytic element (Ni, Pd or Ru) atoms, their energy impact on the individual steps and selectivity. Evaluation of morphological and structural characteristics, and sorption or intrinsic reaction kinetics has indicated that the coverage of acidic sites (on alumina or silica) facilitated yielding ring hydrogenation, inhibited deoxygenation, decarbonylation and cyclic compound opening, and supressed etherification. The rates for aromatics or aldehyde functional groups were, nonetheless, affected in a different order. Understanding the chemistry of bio-based furanic derivatives mechanistically is vital and can improve the process of their conversion into of mono- or di-alcohols.

1. Introduction

In recent decades, ample effort has been devoted to researching renewable and sustainable sources of energy and chemicals. Lignocellulosic biomass has the potential to supplant fossil fuels, which would slow down the global warming and improve the economic independence and in robustness [1]. Cellulose, hemicellulose and lignin are the main components of lignocellulosic biomass, which can be converted using various technologies, such gasification, hydrolysis, pyrolysis, chemical conversion [2]. Furfural is one of the promising platform chemicals, as recognized by the US Department of Energy [3,4]. It is most commonly produced with acidic hydrolysis of hemicellulose, followed by sugar dehydration [5–7]. It can be converted to a wide variety of products or chemicals, replacing their fossil fuel based sources [8–14].

Heterogeneous catalysts have a proven track record in an effective and selective conversion of raw chemicals to desired products. For biomass valorization, Pd, Ru and Ni are particularly useful hydrogenation catalysts, which are used on different supports. Protic solvents, such as water or alcohols (methanol, ethanol, 2-propanol), are most commonly used although aprotic hydrophobic solvents (toluene, octane) have also been occasionally used with varying success [15–17]. It has been shown previously that protic solvents (2-propanol) without gaseous hydrogen perform worse, as evidenced by a slower conversion and formation of side products due to etherification [18].

Pd is particularly known for its ability to selectively hydrogenate C = C bonds without reducing the C = O bond [19]. Pd-based catalysts are generally stable and highly active for hydrogenation and, especially at higher temperatures, for deoxygenation, decarbonylation or ring opening [18–30]. Pd/Al$_2$O$_3$ and Pd/SiO$_2$ catalysts have shown high activity for ring hydrogenation and some aldehyde reduction in water under mild conditions (30 °C, 0.5 MPa H$_2$) [31], with Pd/Al$_2$O$_3$ being more active.

Ru-based catalysts are active especially for hydrogenation but might catalyze decarbonylation and ring opening reactions, depending on the hydrogen/furfural ratio and the Ru particle size [32–36]. In contrast to Pd-based catalysts, SiO$_2$-supported Ru is more active compared to Ru/Al$_2$O$_3$ under similar reaction conditions [31]. Ni stands out as a highly active non-noble metal catalyst for furfural hydrotreatment but is prone

---

* Corresponding author.
  E-mail address: miha.grilc@ki.si (M. Grilc).

to instability and leeching [21,25,30,37–45]. On furfural, Ni/SiO$_2$ and Ni/Al$_2$O$_3$ were particularly active for aldehyde hydrogenation, followed by ring hydrogenation [40,46–48]. Decarbonylation and ring opening, although possible, were observed to a lesser extent [21]. Although research is scarce, both supports (SiO$_2$ and Al$_2$O$_3$) seem to show some activity for furfural hydrotreatment reactions [49–51].

We have previously screened different metals for their catalytic activity in furfural hydrotreatment. Using experiments, first-principles modelling and empirical modelling, we have evaluated Pd/C, Pt/C, Re/C, Ru/C, Rh/C, Ni/C and Cu/C [18,36]. In all cases, only C-supported catalysts were used, focusing our investigation on the active metal effect on neutral support. To quantify their activity, a generalized microkinetic model was developed, which was used descriptively and predictively for the optimization of reaction conditions. In particular: Pd/C was unselective in hydrogenation, reducing both the ring and the aldehyde group (100–200 °C). Ru selectively hydrogenated the aldehyde group at a lower temperature (100 °C) and catalysed decarbonylation and ring opening at higher temperatures (150–200 °C). Ni was selective for the aldehyde group hydrogenation below 150 °C, while at 200 °C decarbonylation occurred. At 212 °C, methylfuran was the main product formed.

Since Ru, Pd and Ni exhibited the highest conversions and varying selectivities depending on the temperature, we have opted to use these three metals to study the support effect in this work. To compare the effects of C, SiO$_2$ and Al$_2$O$_3$ supports, we have synthetized six (Pd/Al$_2$O$_3$, Pd/SiO$_2$, Ru/Al$_2$O$_3$, Ru/SiO$_2$, Ni/Al$_2$O$_3$, Ni/SiO$_2$) catalysts. In-house synthesis was carried out to retain the greatest control on the catalyst composition and to ensure comparability between batches, which would be difficult if using commercial catalysts from different producers.

The experimental data from the temperature-programmed desorption of carbon monoxide (CO–TPD) and ammonia (NH$_3$-TPD) were described with a numerical model to estimate the adsorption and desorption kinetic parameters on metallic and acidic sites. This allowed for the adaptation of a generalized microkinetic model [36], which takes the number of active sites as input when describing the catalyst activity. With this a quantitative distinction between the contributions of metallic sites, active support and the metal-support interactions is featured. The presented results also have direct applicable value, since a wide window of i) various metals, ii) promising supports, iii) temperatures, iv) reaction times has been systematically screened experimentally and well described with relevant kinetic parameters. This allows either empirical or *in silico* (catalyst selection) process optimisation for yielding desired furanics or even diols.

2. Materials and methods

2.1. Materials

All gasses and chemicals were provided by commercial suppliers and used as is: N$_2$ (5.0, Messer, Gumpoldskirchen, Austria), H$_2$ (5.0, Messer, Gumpoldskirchen, Austria), furfural (99 %, Sigma-Aldrich, St Louis, MO, USA, reference number 185914) and tetrahydrofuran for analysis (≥99.8 %, Merck KGaA, Darmstadt, Germany, reference number 1097312500). Catalyst characterization was performed by using 5 % H$_2$ in Ar (Messer, Ruše, Slovenia), helium (5.0 Messer, Bad Soden am Taunas, Germany), carbon monoxide (5 vol% CO in He, Linde, Pullach, Germany), ammonia (5 vol% in He, Linde, Pullach, Germany).

For catalyst synthesis, we used palladium (II) nitrate dihydrate (40 % Pd Basis, Sigma-Aldrich, Saint Louis, MO, USA, reference number 76070), nickel (II) nitrate hexahydrate (≥97 wt%, Sigma-Aldrich, St. Louis, MO, USA, reference number 72253), ruthenium (III) chloride hydrate (35–40 % Ru, Acros organics,New Jersy, USA), silica gel (high-purity grade, pore size 60 Å, 60–100 mesh, reference number 236799), and pure γ-alumina (Spheralite 537, Procatalyse, France), which was crushed and sieved (50–100 mesh) prior use.

2.2. Catalyst preparation

All catalysts were prepared by the incipient wetness impregnation technique. Aqueous solutions of Pd, Ni and Ru salts were used as metal precursors, while silica gel and γ-alumina (crushed and sieved) were used as the supports. Six catalysts were synthetized: Pd/Al$_2$O$_3$, Pd/SiO$_2$, Ru/Al$_2$O$_3$, RuSiO$_2$, Ni/Al$_2$O$_3$, Ni/SiO$_2$. The metal precursor was weighed (calculated as 5 wt% metal in the final catalyst) and dissolved in ultra-pure water (with volume equalling pore volume of support). After incipient wetness impregnation, the catalysts were dried overnight at 110 °C in a furnace to remove water, followed by calcination for 3 h at 500 °C, using a heat up ramp of 5 °C min^{-1}. The catalyst was then slowly cooled to room temperature overnight.

2.3. Catalyst characterization

An X-ray diffraction (XRD) analysis was performed on the fresh and unreduced catalysts by the PANalytical X'Pert PRO instrument with in a 2 ϕ range of 5° to 90° with a 0.001° minimum step size. CuKα (5 kW, 45 mA) was used as radiation source (λ = 0.154056 nm) with a Ni filter for K$_\beta$ radiation.

N$_2$ physisorption measurements were performed on the fresh and unreduced catalysts by the ASAP 2020 gas adsorption instrument (Micrometrics, Norcross, GA, USA). The obtained nitrogen adsorption-desorption isotherms were used to determine the BET specific surface area (S_{BET}), total volume of pores (V_p) and average pore diameter (d_p).

Temperature programmed reduction with hydrogen (H$_2$-TPR), temperature programmed desorption of carbon monoxide (CO–TPD) and temperature programmed desorption of ammonia (NH$_3$–TPD) were performed by the Micrometrics AutoChem II Chemisorption Analyser (Micrometrics, Norcross, GA, USA). Typically, 100 mg of the calcined catalyst was put in a quartz U-tube. The sample was preheated up to 300 °C for 30 min, using a heating rate of 30 °C min^{-1} and 50 mL min^{-1} flow of argon to remove all water. After the sample was cooled down, the catalyst was reduced. A 40 mL min^{-1} flow of 5 vol% of H$_2$ in Ar was introduced and the catalyst was heated up to 400 °C for 3 h with a 10 °C min^{-1} ramp. The sample was afterwards cooled to room temperature with a cooling rate of 20 °C min^{-1}. H$_2$-TPR was performed measuring the hydrogen consumption during the catalyst reduction with a TCD detector.

CO-TPD was performed after the reduction. The sample was flushed with He and saturated with CO, using 5 vol% CO in He at room temperature. The sample was flushed again in a 25 mL min^{-1} flow of He for 30 min and heated up to 800 °C at 10 °C min^{-1}. A MS detector was used to measure CO (28 *m/z*) and CO$_2$ (44 *m/z*) signals in the outlet. The concentration of the desorbed CO was calculated by measuring the baseline during CO saturation (5 vol% CO in He) and after assuming all CO was desorbed (Pure He) using a linear equation.

NH$_3$–TPD was performed after the reduction. The sample was purged with He, followed by NH$_3$ saturation, by using 5 vol% NH$_3$ in He. The sample was flushed again with a 25 mL min^{-1} flow of pure He for 30 min prior to measurement. Afterwards, the sample was heated up to a temperature plateau of 410 °C for 30 min, using a heating rate of 10 °C min^{-1}. The concentration of the desorbed NH$_3$ was calculated measuring the baseline during NH$_3$ saturation (5 vol% NH$_3$ in He) and after assuming all NH$_3$ was desorbed (pure He) using a linear equation.

2.4. Catalyst screening

Catalytic hydro(deoxy)genation tests were performed in a batch three-phase reactor system, consisting of 75 mL reactors (Parr series 5000 multiple reactor system), equipped with sampling tubes. Six different catalysts (Pd/Al$_2$O$_3$, Pd/SiO$_2$, Ru/Al$_2$O$_3$, RuSiO$_2$, Ni/Al$_2$O$_3$, Ni/SiO$_2$) were tested at 150 °C, 175 °C and 200 °C, as shown in Table 1. Prior to reaction, all catalysts had been reduced at 400 °C for 4 h in a tube furnace under a 200 mL min^{-1} hydrogen flow, cooled down and

Table 1

Experimental conditions during catalytic screening with 0.2 wt% catalyst and 5 wt% furfural in tetrahydrofuran under 60 bar H_2 and stirring at 1000 rpm.

Experiment	Catalyst/support	T_{final} (°C)
1	Al_2O_3	200
2	SiO_2	200
3	Pd/SiO_2	150
4	Pd/Al_2O_3	150
5	Ru/SiO_2	150
6	Ru/Al_2O_3	150
7	Ni/SiO_2	150
8	Ni/Al_2O_3	150
9	Pd/SiO_2	175
10	Pd/Al_2O_3	175
11	Ru/SiO_2	175
12	Ru/Al_2O_3	175
13	Ni/SiO_2	175
14	Ni/Al_2O_3	175
15	Pd/SiO_2	200
16	Pd/Al_2O_3	200
17	Ru/SiO_2	200
18	Ru/Al_2O_3	200
19	Ni/SiO_2	200
20	Ni/Al_2O_3	200

carefully transferred in an inert atmosphere into the reaction mixture.

A typical reaction mixture consisted of 0.2 wt% of a catalyst, 5 wt% of furfural and 94.8 wt% of tetrahydrofuran. The reactor was flushed with nitrogen before 60 bar H_2 was introduced (at room temperature) to ensure that excess hydrogen was available (desired molar ratio H_2: furfural is approximately 5 to 1). Under vigorous stirring (1000 rpm with a magnetic stirring bar), the reaction mixture was heated up (a ramp of 5 – 9 °C min^{-1}) to reach the set temperature fast (ideally in 25 min). On-line temperature and pressure measurements were performed during each experiment. After the reaction, the reactor was cooled down and flushed with nitrogen.

2.5. Sample analysis

During the catalytic experiment, the liquid phase was sampled sequentially at regular time intervals. The first and last sample were collected prior to the introduction of hydrogen and after the reactor cooldown, respectively. For analysis with a gas chromatograph with flame ionization detector (Thermo Fisher Scientific, Waltham, MA, USA), coupled with mass spectrometer detector (2010 Ultra, Shimadzu, Kyoto, Japan) (GC-FID/MS), the samples had to be diluted 25-fold in tetrahydrofuran. The FID detector was used for quantification. The MS signal was used for identification and quantification of tetrahydrofurfural (71 m/z signal) and furfural (67 m/z signal), where the peaks overlapped in the FID chromatogram (using 2,6–di–tert–butyl–4–methylphenol (BHT) was used as internal standard).

2.6. Distinguishing between the metallic and acidic sites using temperature programmed desorption

TPD experiments were used to obtain information on the abundance and type of active sites on the catalyst surface. In particular, we can calculate the number of active sites, initial surface coverage and adsorption/desorption energy along with the corresponding rate constants. CO-TPD was used to determine the metallic (M) sites and NH_3-TPD for acidic/support (Ac) sites.

To model the experimental data a previously developed fixed-bed reactor model [36] was modified. As shown in Eqs. (1) and (2) for CO and Eqs. (3) and (4) for NH_3, TPD is modelled as a dynamic equilibrium between the adsorption and desorption in a gas flow along the reactor, where TPD experiments took place. The adsorption is a kinetic effect (non-activated event), which is roughly independent of the temperature,

while desorption is strongly dependent on the temperature because the adsorption interaction must be overcome (it follows the Arrhenius kinetics in the first approximation). In modelling, we are solving the molar balance equations:

$$\frac{\partial C_{CO}}{\partial t} = -v \bullet \frac{\partial C_{CO}^g}{\partial x} - k_{ads}^{CO,M} \bullet C_{CO}^g(x) \bullet \left(1 - \theta_{CO}^M(x)\right) + k_{des}^{CO,M}(T) \bullet \theta_{CO}^M(x)$$
$$\bullet \frac{n_M}{V_{gas}} \tag{1}$$

$$\frac{\partial \theta_{CO}^M(x)}{\partial t} = k_{ads}^{CO,M} \bullet C_{CO}^g(x) \bullet \left(1 - \theta_{CO}^M(x)\right) \bullet \frac{V_{gas}}{n_M} - k_{des}^{CO,M}(T) \bullet \theta_{CO}^M(x) \tag{2}$$

or

$$\frac{\partial C_{NH_3}}{\partial t} = -v \bullet \frac{\partial C_{NH_3}^g}{\partial x} - k_{ads}^{NH_3,Ac} \bullet C_{NH_3}^g(x) \bullet \left(1 - \theta_{NH_3}^{Ac}(x)\right) + k_{des}^{NH_3,Ac}(T)$$
$$\bullet \theta_{NH_3}^{Ac}(x) \bullet \frac{n_{Ac}}{V_{gas}} \tag{3}$$

$$\frac{\partial \theta_{NH_3}^{Ac}(x)}{\partial t} = k_{ads}^{NH_3,Ac} \bullet C_{NH_3}^g(x) \bullet \left(1 - \theta_{NH_3}^{Ac}(x)\right) \bullet \frac{V_{gas}}{n_{Ac}} - k_{des}^{NH_3,Ac}(T) \bullet \theta_{NH_3}^{Ac}(x) \tag{4}$$

Initial conditions ($t = 0$) were defined as follows: the gaseous concentration of CO at the inlet ($x = 0$) is zero, and CO surface coverage is 1. Plug-flow concentration and velocity profile of gases was considered through the void in the catalyst bed in axial direction, with no preferenced flow path (channeling) and no-axial dispersion considered, as well as no channeling. Zero concentration gradients has been set as boundary conditions before the inlet and at the outlet of the catalytic zone. The He flow rate was set to 25 cm^3 min^{-1} at ambient conditions and was corrected for temperature expansion using the ideal gas law, where isothermal temperature profile of the space domain was assumed for every time step. Solving for the surface coverage (θ_{CO}^M, $\theta_{NH_3}^{Ac}$) and gas phase concentration (C_{CO}^g, $C_{NH_3}^g$) the total number of metallic and acidic sites (n_M, n_{Ac}), adsorption/desorption rate constants ($k_{ads}^{CO,M}$, $k_{ads}^{NH_3,Ac}$ and $k_{des}^{CO,M}(T)$, $k_{des}^{NH_3,Ac}(T)$), and activation energy of desorption ($E_{CO}^{des,M}$ and $E_{NH_3}^{des,Ac}$).

The ensuing partial differential equations were defined as a set of ordinary differential equations for every x-dimension-step and solved using the ode15s solver in Matlab. TPD profiles for each tested catalyst were obtained by fitting ($\theta_{CO}^M(t = 0)$), n_M, $k_{ads}^{CO,M}$, $k_{des}^{CO,M}(T)$,) or ($\theta_{NH_3}^{Ac}(t = 0)$), n_{Ac}, $k_{ads}^{NH_3,Ac}$, $k_{des}^{NH_3,Ac}$) at 150 °C and $E_{CO}^{des,M}$ and $E_{NH_3}^{des}$ to the experimental data, using the Nelder-Mead method with the objective function defined as a sum of squared residuals. The concentration of active sites (C_M or C_{Ac}) was defined per mass ($\frac{n_M}{m}$, $\frac{n_{Ac}}{m}$). The obtained sorption parameters based on the contribution from both metallic sites and acidic sites were used in the microkinetic model, as described in supplementary data and based on the framework presented in our previous work Ref. [36].

2.7. Surface reactions

2.7.1. Reaction pathway

Furfural can be ultimately hydrogenated to methyltetrahydrofuran (MTHF). Depending on the reaction pathway, namely the preference of the aromatic ring or aldehyde group for hydrogenation, different intermediates are formed in the process, as shown in Fig. 1 and further explained in Ref [36]. The products of partial hydrogenation (FA, THFUR), full hydrogenation (THFA), deoxygenation (MF, MTHF) and ring opening (OR), such as pentan-1-ol and pentan-2-ol, were observed experimentally. Furfural can undergo aldehyde group hydrogenation (k_1), followed by ring hydrogenation (k_4), or vice-versa (k_2, k_3). Deoxygenation of the hydroxyl group (k_5, k_6) can follow, while the
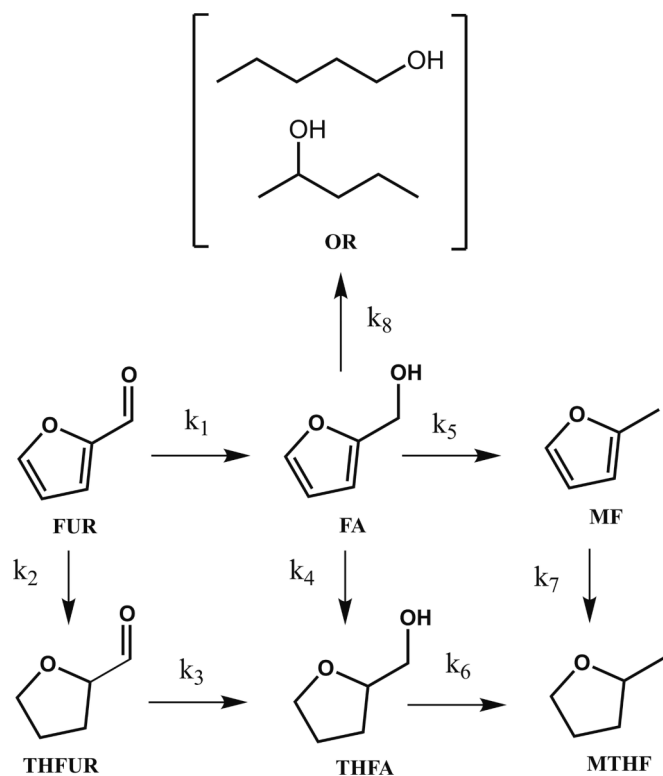
Fig. 1. Proposed reaction pathway for furfural hydrotreatment on the tested catalysts. Adapted from Ref. [36].

deoxygenated product MF can also be fully hydrogenated (k_7). It was assumed that OR products can mostly form from FA. Products, observed in low quantities, were neglected.

2.7.2. Modelling

The generalized microkinetic model, developed in Ref. [36] was expanded to include the decoupled contributions of both types of active sites (M and Ac). As negligible reaction activity over pure supports was observed, only adsorption and desorption over acidic sites in addition to reaction kinetics, adsorption and desorption over metallic sites was taken into account. Reaction kinetics over acidic sites was neglected due to lack of their direct activity. Due to large differences between the kinetics, observed over catalysts, containing the same active metal (Pd, Ru or Ni), each catalyst had to be fitted separately. Firstly, reaction rate constants over metallic sites were obtained by fitting the experimental data at 175 °C, for each tested catalyst (Pd/SiO$_2$, Ru/SiO$_2$ and Ni/SiO$_2$, Pd/Al$_2$O$_3$, Ru/Al$_2$O$_3$ and Ni/Al$_2$O$_3$). Knowing the reaction rates at 175 °C, the activation energies were determined from fitting to different temperatures. Hydrogen mass transport was assumed not to limit the reaction rates due to rapid steering and almost pure hydrogen in the gas phase. It was shown previously that reaction rates are not limited due to sufficiently large hydrogen gas-liquid transfer parameters ($k_l a_g$). [18,36] The model assumes that (i) the initial H$_2$ pressure equals the total pressure in the reactor vessel, (ii) hydrogen solubility in THF can be described by Henry's law, (iii) surface reactions follow the Lagmuir-Hinshelwood mechanism, and (iv) adsorption/desorption is competitive. It was additionally assumed, that the activity of the support did not change with varying active metal depositions. Adsorption and desorption parameters were estimated in the TPD simulations.

Surface reactions, *i*, involving hydrogen, species *j* were modelled as:

$$r_i(t, T) = k_i(T)\theta_j(t)\theta_{H_2}(t) \tag{5}$$

while adsorption and desorption are modelled as

$$r_j^{ads}(t, T) = k_j^{ads}(T)C_j(t)\theta_{\text{vacant}}(t) \tag{6}$$

$$r_j^{des}(t, T) = k_j^{des}(T)\theta_j(t)$$

Reaction rate constants, k_i, and desorption rate constants k_j^{des} are calculated according to the Arrhenius formalism (Eq. (7)). The overall list of the kinetic and mass balance equations (S1-S83) can be found in the SI. For further details on the model, please see Refs. [18,36].

A set of ordinary differential equation was solved with the ode15s solver in Matlab. The Nelder–Mead method was used for regression analysis with a sum of squared residuals as the objective function.

$$k_i(T) = k_i(T_{\text{ref}})\exp\left(\left(-\frac{E_{a,i}}{R}\right)\left(\frac{1}{T} - \frac{1}{T_{\text{ref}}}\right)\right) \tag{7}$$

3. Results and discussion

3.1. Catalyst characterization

Based on N$_2$ physisorption measurements, all catalysts exhibited mesoporous structure (Fig. S1). As shown in Table 2, SiO$_2$-supported catalysts exhibited roughly three times greater surface area, 1.6 times greater pore volume and 2 times smaller average pore diameter, compared to Al$_2$O$_3$ supported catalysts, which is also the case for pure (non-loaded) supports. The catalysts have similar morphology properties as their parent supports. It appears that the metal deposition did not meaningfully change the texture or block the pores. Furthermore, we can assume that adsorption/desorption and kinetic properties of the support (acidic) sites do not change noticeably upon metal deposition.

XRD analysis showed no visible change in the bulk structure of the support after metal deposition (Fig. S2). The crystalline structure of Pd and Ru seems similar on both SiO$_2$ and Al$_2$O$_3$ supports, although the peak intensity seems slightly higher for Ru/Al$_2$O$_3$ compared to Ru/SiO$_2$. This is in accordance with CO-TPD results and further elaborated in Section 3.3. Nevertheless, NiO peaks are broader in Ni/Al$_2$O$_3$, compared to those in Ni/SiO$_2$, which hints at a higher dispersion of NiO and/or stronger interaction between NiO and Al$_2$O$_3$ [52].

H$_2$-TPR was performed to estimate the catalyst reducibility as all catalysts were reduced at 400 °C for 3 h prior to catalytic tests. Although no clear Pd reduction peak was observed (Fig. S3), it is known that Pd can be reduced at low temperatures. Since both Pd/Al$_2$O$_3$ and Pd/SiO$_2$ are reducible at 80 °C, Pd must have been already reduced during the H$_2$ flushing step before heating [53,54]. A clear reduction was observed for Ru/Al$_2$O$_3$ and Ru/SiO$_2$ between 90 and 200 °C. Ni/SiO$_2$ showed a broad reduction peak between 270 °C and 400 °C, while barely noticeable reduction was observed over Ni/Al$_2$O$_3$. With Ni being a non-noble metal, NiO is not wholly reduced at or below 400 °C due to its strong interaction with the Al$_2$O$_3$ support (forming NiAl$_x$O$_y$), shifting the required reduction temperature higher [55].

3.2. Liquid phase

Only species shown in Fig. 1 were formed in meaningful amounts.

Table 2
Surface properties of pure supports and catalysts.

Catalyst	S_{BET} (m^2 g^{-1})	V_{p} (cm^3 g^{-1})	d_{p} (nm)
Al$_2$O$_3$	187.2	0.48	10.3
SiO$_2$	556.2	0.76	5.5
Pd/Al$_2$O$_3$	183.0	0.47	10.2
Pd/SiO$_2$	468.8	0.71	6.0
Ru/Al$_2$O$_3$	177.7	0.44	10.0
Ru/SiO$_2$	466.3	0.71	6.1
Ni/Al$_2$O$_3$	162.7	0.45	11.0
Ni/SiO$_2$	476.3	0.73	6.2

The OR products, mostly 1-pentanol, were detected only when using Pd/Al2O3 and Ru/Al2O3. A small amount of 2-pentanol was detected at 200 °C over Pd/Al2O3. Similarly, MTHF was only produced over Pd/Al2O3 (minuscule amounts also over Ru/Al2O3 at 200 °C). MF or furfural oligomers were not detected in meaningful amounts in any experiment. Decarbonylation products, such as THF or furan, could have potentially formed during these reactions, however, would have been masked by the solvent on the chromatographs. Subsequent gas phase analysis ruled out their formation, which is in agreement with our previous work [36]. Decarbonlyation is reported to occur above 200 °C [19].

3.3. CO adsorption on metallic sites

Experimental CO-TPD profiles (shown in Fig. 2) were modelled for
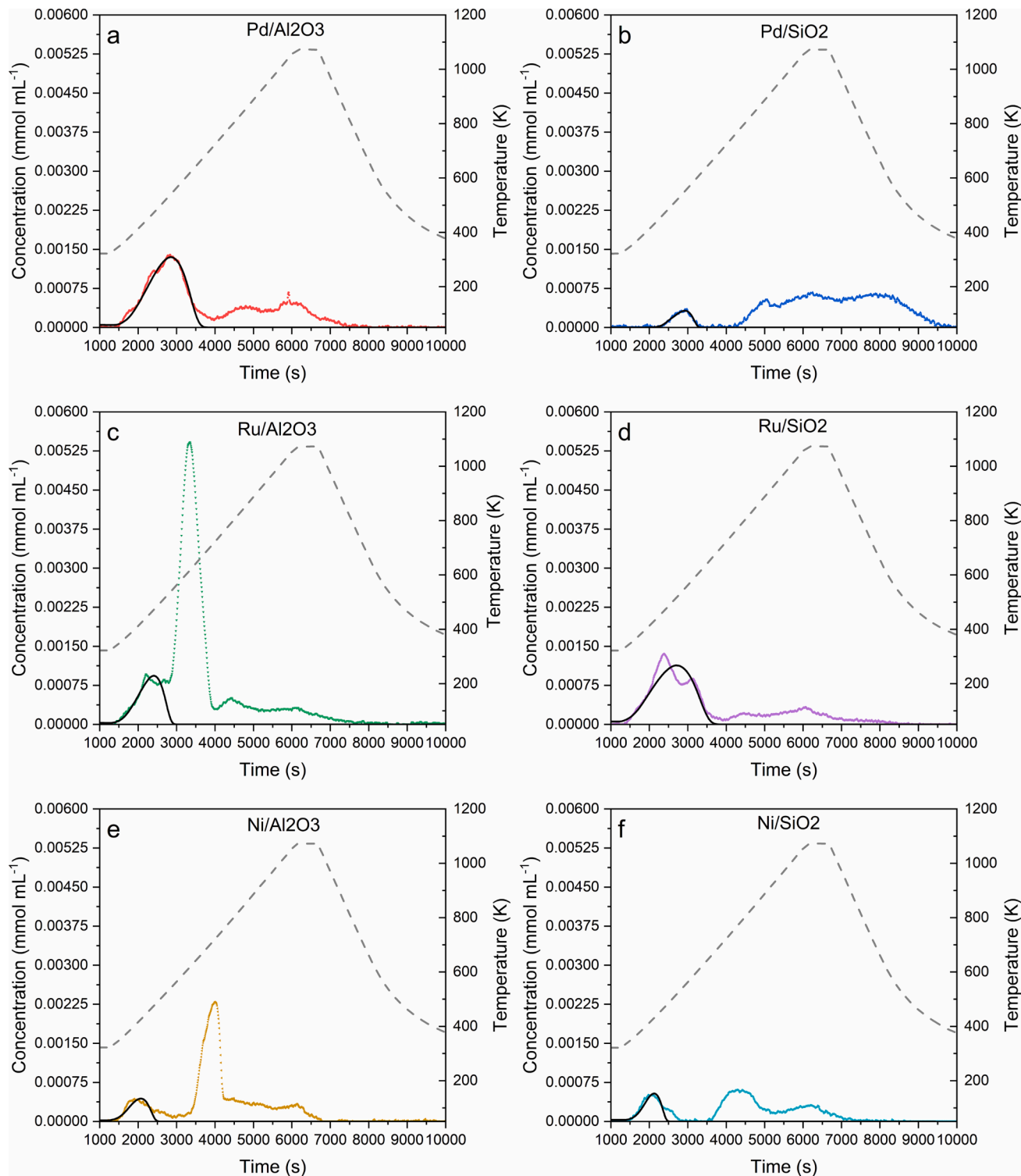
Fig. 2. CO-TPD profiles for a) Pd/Al2O3, b) Pd/SiO2, c) Ru/Al2O3, d) Ru/SiO2, e) Ni/Al2O3 and f) Ni/SiO2. Points, dashed lines and black solid lines represents experimental data, the temperature and fitted model data, respectively. Only TPD peaks below the maximum reaction temperature (200 °C) were considered relevant and thus, were included in the kinetic model.

each tested catalyst to estimate the parameters, which are summarized in Table 3: CO desorption rate constants at 150 °C ($k_{CO}^{des,M}$), activation energy of desorption ($E_{CO}^{des,M}$) and the total number of metallic surface sites (n_M). The CO adsorption rate constant ($k_{CO}^{ads,M}$) was set to $1.7 \bullet 10^8$ s^{-1} and kept temperature-independent, as shown in Ref [36]. We assumed that one mole of desorbed CO is equivalent to one mole of active metal surface sites n_M. The initial metallic surface coverage ($\theta_{CO}^M(t = 0)$) was allowed to be less than 1 to account for desorption of the weakly adsorbed CO during the flushing of the catalyst prior to heating (due to different types of metallic sites, see below). Varying initial surface coverages does not change the kinetic parameters of the CO adsorption desorption, as long as the coverages are not unreasonably low [36]. The pre–exponential of the reaction rate constant ($A_{CO}^{des,M}$) was estimated from the Arrhenius equation, using $k_{CO}^{des,M}(T = 150 °C)$ and $E_{CO}^{des,M}$.

As seen in Fig. 2, most catalysts exhibit multiple desorption peaks for CO-TPD, which can be due to the deposited metals, support, bimetallic surfaces and their various interactions. However, only the adsorption sites, which can be vacated below the temperature of the reaction (200 °C), are relevant. Hence, modelling took into account the weaker adsorption sites, which are responsible for the kinetic activity below 200 °C. The desorption peaks at higher temperatures are either the result of strong support–metal interactions or surface sites found on the pure support, as these peaks were not found on single metal catalysts (Pd/C, Ru/C, Ni/C) [36].

Table 3 shows that the c_M values differ as different surface sites density were formed. Results match well with the XRD data (Fig. S2), as metallic surface sites density is higher for Ru/SiO$_2$ ($8.4 \bullet 10^{-6}$ g/mol) compared to Ru/Al$_2$O$_3$ ($4.7 \bullet 10^{-6}$ g/mol), which corresponds to stronger and sharper XRD signal of larger Ru crystallites on alumina compared to silica. Contrarily, Pd dispersion over Al$_2$O$_3$ is higher compared to SiO$_2$, which also matches with the trend on diffractograms. Table 3 also shows that selection of the support changes the desorption properties of the metallic sites considerably, seen as a shift in desorption peaks on TPD profile (Fig. 2) and reflected in desorption parameters ($k_{CO}^{des,M}$, $E_{CO}^{des,M}$). Finally, desorption rates are temperature-sensitive as a result of relatively high $E_{CO}^{des,M}$, especially for Pd/SiO$_2$. Desorption parameters from Table 3 were used in the microkinetic model to describe the sorption properties of metallic sites.

3.4. NH$_3$ adsorption on acidic (support) sites

The kinetic model for TPD-NH$_3$ was developed analogously to describe and characterise the acidic (support) sites. Due to the basicity of NH$_3$, its adsorption was assumed to occur exclusively on acidic sites found on the support (Al$_2$O$_3$ or SiO$_2$). One mole of adsorbed NH$_3$ was assumed to be equivalent to one mole of acidic sites. The fitted desorption parameters are shown in Table 4.

Comparing the concentration of active metal sites (Table 3) with the

Table 4
Acidic sites parameters from modelling the NH$_3$-TPD experiments.

Parameter	Pd/ Al$_2$O$_3$	Pd/ SiO$_2$	Ru/ Al$_2$O$_3$	Ru/ SiO$_2$	Ni/ Al$_2$O$_3$	Ni/ SiO$_2$
c_{Ac} [mol g^{-1}]	$2.6 \bullet 10^{-4}$	$5.2 \bullet 10^{-5}$	$2.5 \bullet 10^{-4}$	$3.5 \bullet 10^{-5}$	$3.0 \bullet 10^{-4}$	$8.2 \bullet 10^{-5}$
$\theta_{NH_3}^{Ac}(t = 0)$ [/]	0.74	0.43	0.69	0.63	0.77	0.34
$k_{NH_3}^{des,Ac\ a}$ [s^{-1}]	$4.7 \bullet 10^3$	$9.0 \bullet 10^3$	$7.0 \bullet 10^3$	$7.8 \bullet 10^3$	$3.9 \bullet 10^3$	$1.1 \bullet 10^4$
$A_{NH_3}^{des,Ac}$ [s^{-1}]	$2.0 \bullet 10^6$	$9.7 \bullet 10^4$	$4.1 \bullet 10^6$	$7.6 \bullet 10^5$	$1.4 \bullet 10^6$	$2.7 \bullet 10^5$
$E_{NH_3}^{des,Ac}$ [kJ mol^{-1}]	21.2	8.4	22.4	16.1	20.6	11.4

* Temperature-dependent. Evaluated at 150 °C.

concentration of acidic sites (Table 4), we see that the concentration of acidic sites is approximately one (Al$_2$O$_3$) or two (SiO$_2$) orders of magnitude larger. Al$_2$O$_3$-supported catalysts have up to 3 overlapping peaks each (3 different types of acidic sites) with different intensities, while all SiO$_2$ supported catalysts look similar and have multiple overlapping peaks (Fig. 3). Nevertheless, the deposition of metal (Pd, Ru or Ni) did not meaningfully change the average acidity of either Al$_2$O$_3$ or SiO$_2$ support, although small differences in c_{Ac} and desorption parameters can be found. The deposition of the metal during the catalyst synthesis can block some catalyst pores or be deposited directly on acidic sites found on support. Desorption parameters (Table 4) for either Al$_2$O$_3$- or SiO$_2$-supported catalysts differ only slightly. The adsorption and desorption kinetics on acidic sites are fairly insensitive to the change in temperature (evidenced by low $E_{NH_3}^{des,Ac}$).

3.5. Furfural hydrotreatment

3.5.1. Acidic sites

Experiments (Entry 1 and 2 in Table 1) with pure Al$_2$O$_3$ and SiO$_2$ supports showed no measurable catalytic activity at 200 °C. Hence, it was assumed that the acidic sites alone cannot be directly responsible for the catalytic activity. As the experimental characterisation found no significant changes of the support upon metal loading, it is believed not to effect any change in the activity.

However, in conjunction with the active metal, supports are not inert but instead provide additional adsorption sites that influence the adsorption/desorption equilibria. While it is unlikely that the studied reactions are adsorption-limited, which is also assumed in our kinetic model, a change in the number or quality of active sites does influence the reaction rates. Also, no general trend was observed by comparing the activity of the catalysts and the concentration of the acidic sites. Thus, an interaction between the support (Al$_2$O$_3$ or SiO$_2$) and each deposited metal is likely the cause for the variability observed in the resulting catalyst activity and product selectivity.

3.5.2. Metallic sites

A negligible activity of pure supports hints at an interaction between the support and the deposited metal, since the products formed on Al$_2$O$_3$ and SiO$_2$ supported catalysts (see Figs. 5–7) differed when the same metal (Pd, Ru or Ni) was used. The interaction not only affected the overall reaction rate but also the selectivity. This is attributed to the modification of surface sites and change in the electronic structure of the deposited metal as a result of the metal-support interaction, which also affects the size of the deposited metal particles. Thus, the parameters for the reactions occurring on the active metal sites had to be obtained for each catalyst individually. Relatively low number of reactions (8) were considered for description of a relatively large number of experimental points (>750 in total) in order to prevent any over-parametrisation of the model. On the other hand, this resulted in a mediocre agreement

Table 3
Metallic active sites parameters from modelling the CO-TPD experiments.

Parameter	Pd/ Al$_2$O$_3$	Pd/ SiO$_2$	Ru/ Al$_2$O$_3$	Ru/ SiO$_2$	Ni/ Al$_2$O$_3$	Ni/ SiO$_2$
c_M [mol g^{-1}]	$9.4 \bullet 10^{-6}$	$1.1 \bullet 10^{-6}$	$4.7 \bullet 10^{-6}$	$8.4 \bullet 10^{-6}$	$2.0 \bullet 10^{-6}$	$2.3 \bullet 10^{-6}$
$\theta_{CO}^M(t = 0)$	0.92	0.90	0.90	0.89	0.79	0.75
$k_{des}^{CO,M*}$ [s^{-1}]	$2.7 \bullet 10^3$	$4.1 \bullet 10^2$	$1.1 \bullet 10^4$	$2.8 \bullet 10^3$	$3.8 \bullet 10^4$	$9.4 \bullet 10^4$
$A_{CO}^{des,M}$ [s^{-1}]	$9.4 \bullet 10^7$	$6.1 \bullet 10^{12}$	$6.8 \bullet 10^9$	$2.2 \bullet 10^7$	$1.7 \bullet 10^{10}$	$1.5 \bullet 10^{11}$
$E_{CO}^{des,M}$ [kJ mol^{-1}]	36.8	82.3	47.1	31.6	45.7	50.3

* Temperature-dependent. Evaluated at 150 °C.

Fig. 3. NH$_3$-TPD profiles for a) Pd/Al$_2$O$_3$, b) Pd/SiO$_2$, c) Ru/Al$_2$O$_3$, d) Ru/SiO$_2$, e) Ni/Al$_2$O$_3$ and f) Ni/SiO$_2$. Points, dashed lines and black solid lines represents experimental data, the temperature and fitted model data, respectively. Only the peaks below the maximum reaction temperature (200 °C) are relevant during the reaction and thus included in the modelling.
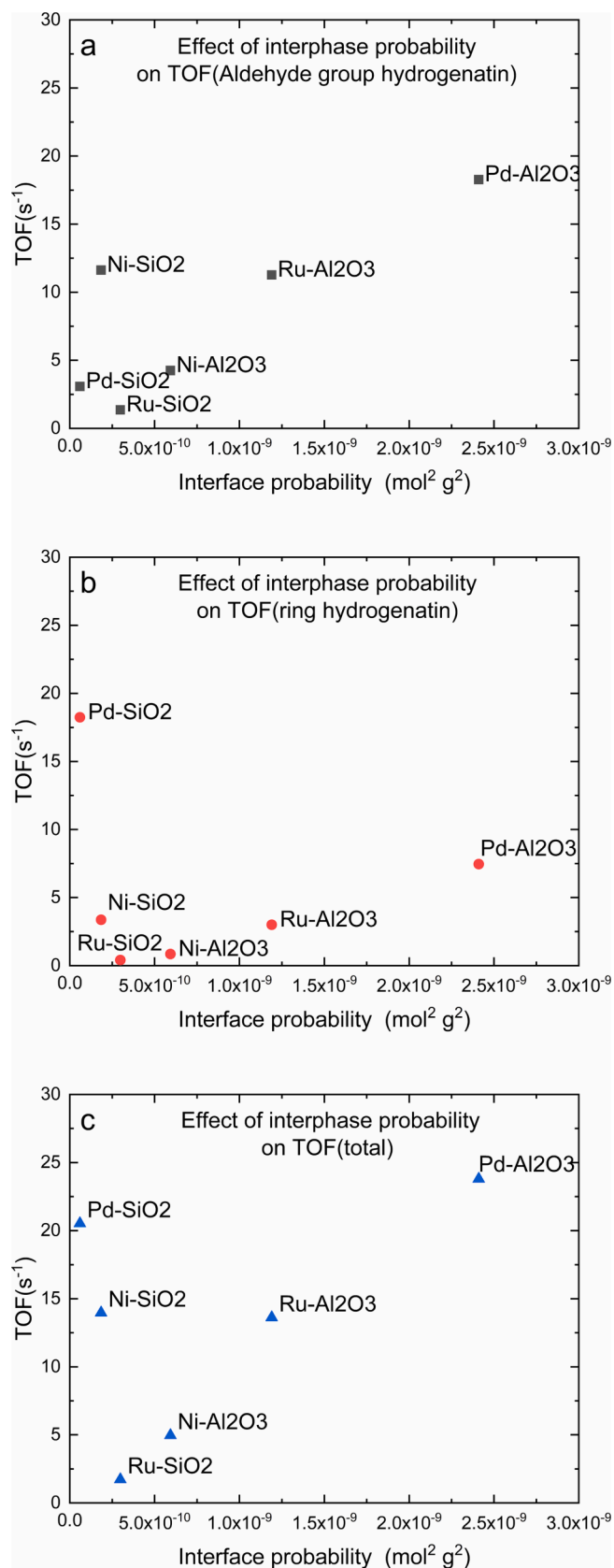
Fig. 4. The role of acidic and metallic sites interphase on the turnover frequencies (TOF) at 175 °C for a) aldehyde group hydrogenation reactions, b) ring hydrogenation reactions and c) overall reactions.

between modelled and experimental values for some experiments (Figs. 5–7), while globally a relatively good agreement and decent parameter reliability was achieved.

The model parameters (Table 5) show that Pd, Ru and Ni performed the aldehyde group hydrogenation (k_1^M and k_3^M) and furfural ring hydrogenation (k_2^M) with either support, while the furfuryl alcohol ring hydrogenation (k_4^M) occurred predominantly on Pd/Al$_2$O$_3$. Some decarbonylation (k_6^M) of THFA and ring opening (k_8^M) towards (mostly) 1–pentanol was also only observed over Pd and Ru when supported on Al$_2$O$_3$. Contrarily, these two reaction pathways were not favoured by the use of support, as acidic sites (scarce on SiO$_2$ based on Table 4) facilitate electrophilic reactions (proceeding on C = C bonds). Upon partial hydrogenation ring opening becomes feasible.

3.5.3. Interphase between acid and metallic sites

To model the effect of the metal-support interaction, the interphase must be quantified. We define the interphase *probability* as a product of the number of acidic sites (Table 4) and metallic sites (Table 3) for each catalyst separately. It is to be noted that this does not represent the *number* of interphase sites but the probability quantity, which can be viewed as an upper bound to be used in the reaction rate expressions.

The interphase probability was then compared to the cumulative TOF values, calculated as a product of the maximum TOF values for individual reactions at 175 °C for the a) aldehyde group hydrogenation reactions (TOF$_1$ + TOF$_3$), b) ring hydrogenation reactions (TOF$_2$ + TOF$_4$) and c) overall cumulative reactions (TOF$_{total}$), as shown in Fig. 4. The reader is referred to Table S1 for the interphase probabilities and cumulative TOF values at all tested temperatures.

We observe that Al$_2$O$_3$ is more acidic compared to SiO$_2$ (having more measurable acidic sites), resulting in a generally higher interphase probability. The cumulative TOF for all three groups of reactions increased with interphase probability over Al$_2$O$_3$ supported catalysts (Pd/Al$_2$O$_3$ > Ru/Al$_2$O$_3$ > Ni/Al$_2$O$_3$), while it decreased over SiO$_2$ supported ones (Ni/SiO$_2$ > Ni/SiO$_2$ > Ru/SiO$_2$). It is known that Al$_2$O$_3$ has generally stronger interactions with deposited metals [55], making it more likely to form bifunctional sites at the interphase, which can also be seen from CO-TPD results (Fig. 2). These bifunctional sites cause the difference in the kinetic parameters between the Al$_2$O$_3$ and SiO$_2$ supported catalysts with the same deposited metal. Ru and Pd supported on Al$_2$O$_3$ showed a higher activity compared to SiO$_2$, hinting at a synergistic effect of the larger interphase in these cases.

However, Ni/SiO$_2$ was found to be more active compared to Ni/Al$_2$O$_3$ despite having a lower concentration of acidic sites, which is explained by the formation of NiAl$_x$O$_y$ [55] during catalyst synthesis, which has an agonistic effect on the Ni/Al$_2$O$_3$ activity. This is corroborated by the higher reduction temperature of Ni/Al$_2$O$_3$, measured during H$_2$-TPR, as shown in Fig. S3.

In contrary to the Al$_2$O$_3$ supported catalysts, the activity of the SiO$_2$ supported catalysts was found to be higher at *lower* interphase probabilities. SiO$_2$ is believed to influence the adsorption and the orientation of furanic species by electrostatic repulsion. Hence, it is preferable to minimize the amount of interphase sites, when using SiO$_2$ as support.

3.5.4. Overall catalyst activity

The Pd/Al$_2$O$_3$ catalyst exhibited a high ring and aldehyde group hydrogenation activity, resulting in total hydrogenation and the forming of THFUR (84 % yield at 200 °C) as the main product at all tested temperatures. In addition to the hydrogenation products, MTHF was also formed in small quantities, while trace amounts of OR (mainly 1-pentanol) were found (See Table S2. for details on conversion, selectivity and yields). As no MF was detected in any experiment, we suggest this reaction to occur through decarbonylation of THFUR rather than FA. Low activation energies for hydrogenation reactions (Table 5) also suggest that the change in reaction temperature does not meaningfully change the reaction activity (although it changes adsorption/desorption
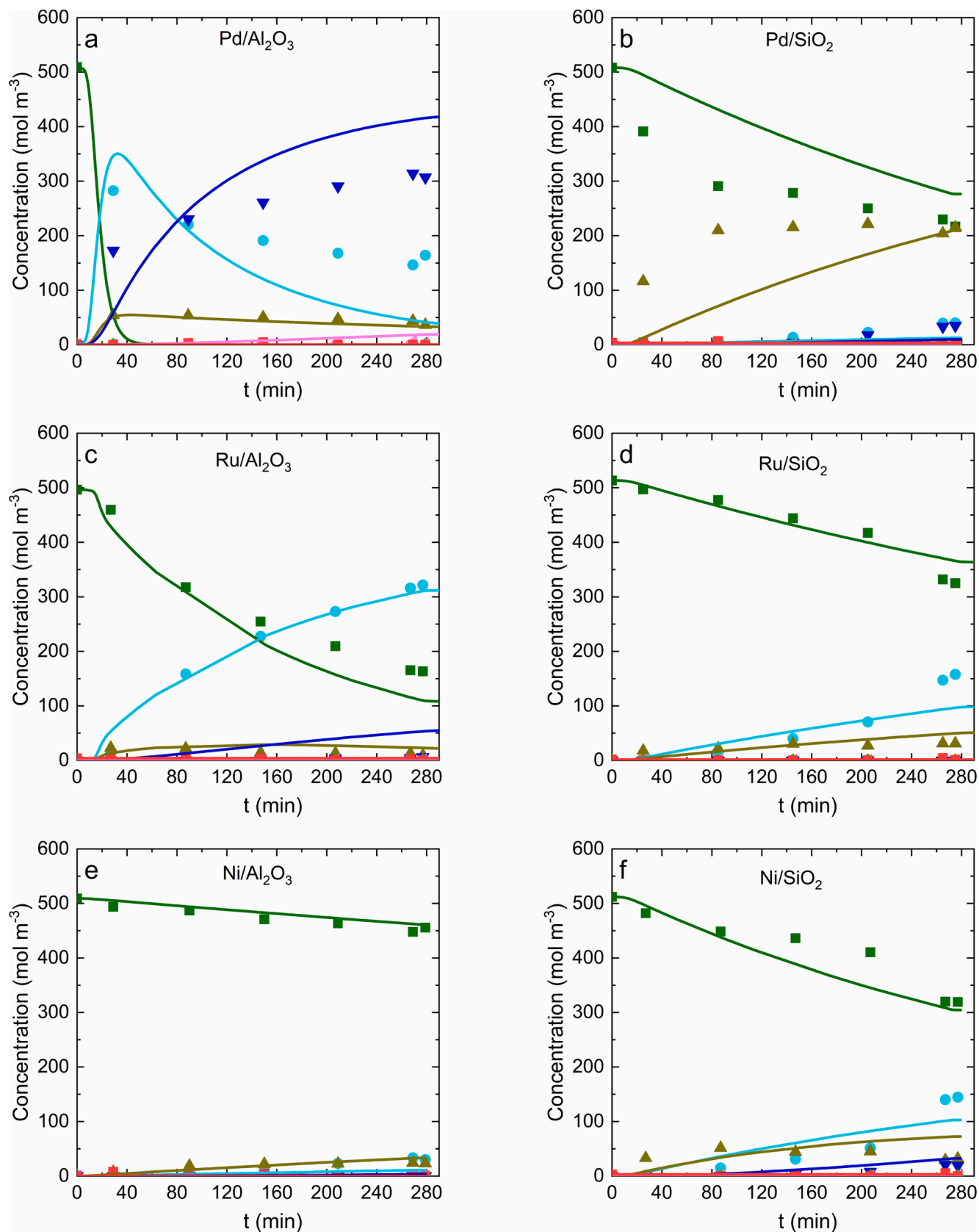
Fig. 5. Kinetic screening at 150 °C. 60 bar of pure hydrogen, 0.2 wt% of catalyst and 5 wt% of furfural mixed in tetrahydrofuran were used. FUR, FA, THFUR, THFA, MF, MTHF, OR.
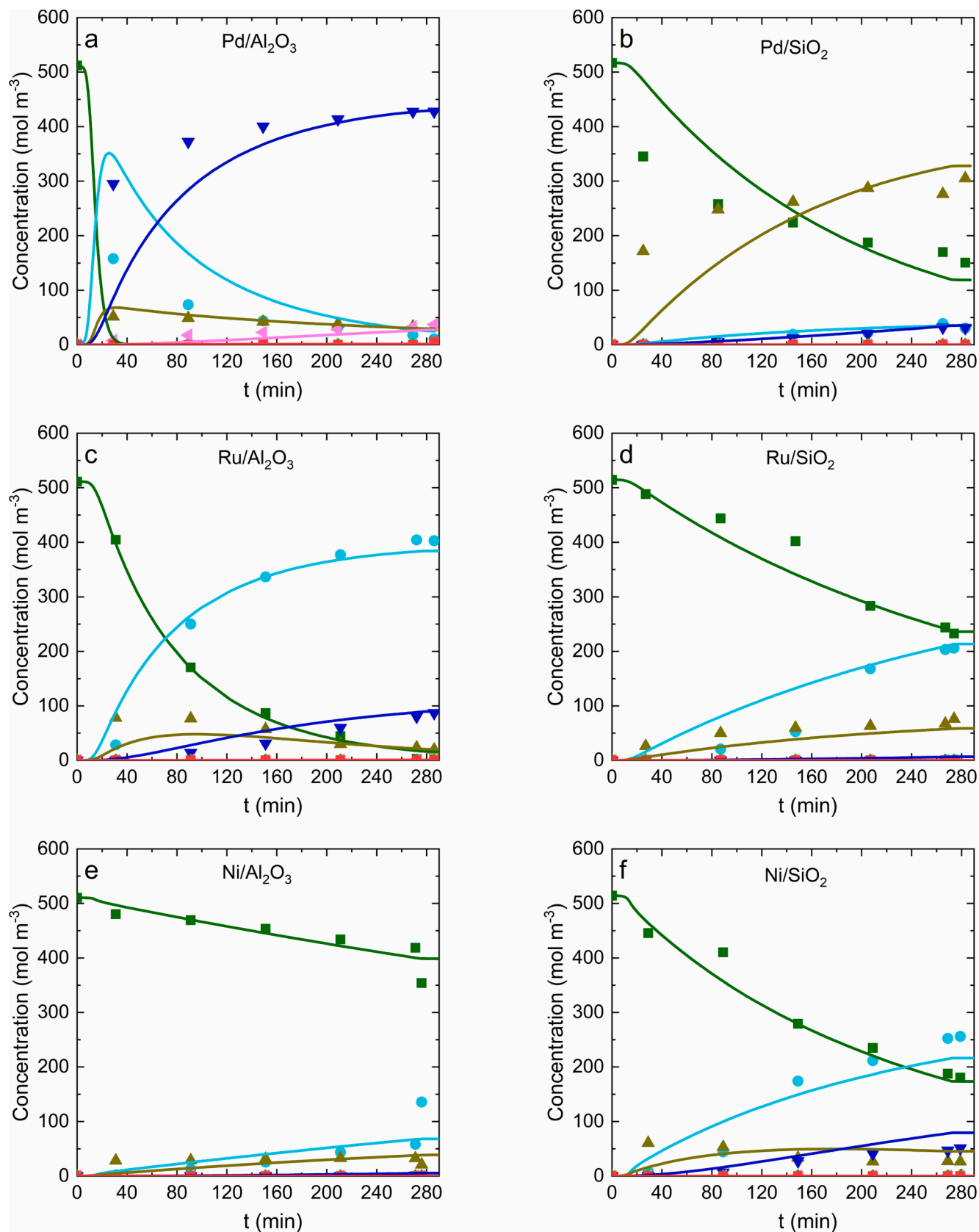
Fig. 6. Kinetic screening at 175 °C. 60 bar of pure hydrogen, 0.2 wt% of catalyst and 5 wt% of furfural mixed in tetrahydrofuran were used. FUR, FA, THFUR, THFA, MF, MTHF, OR.
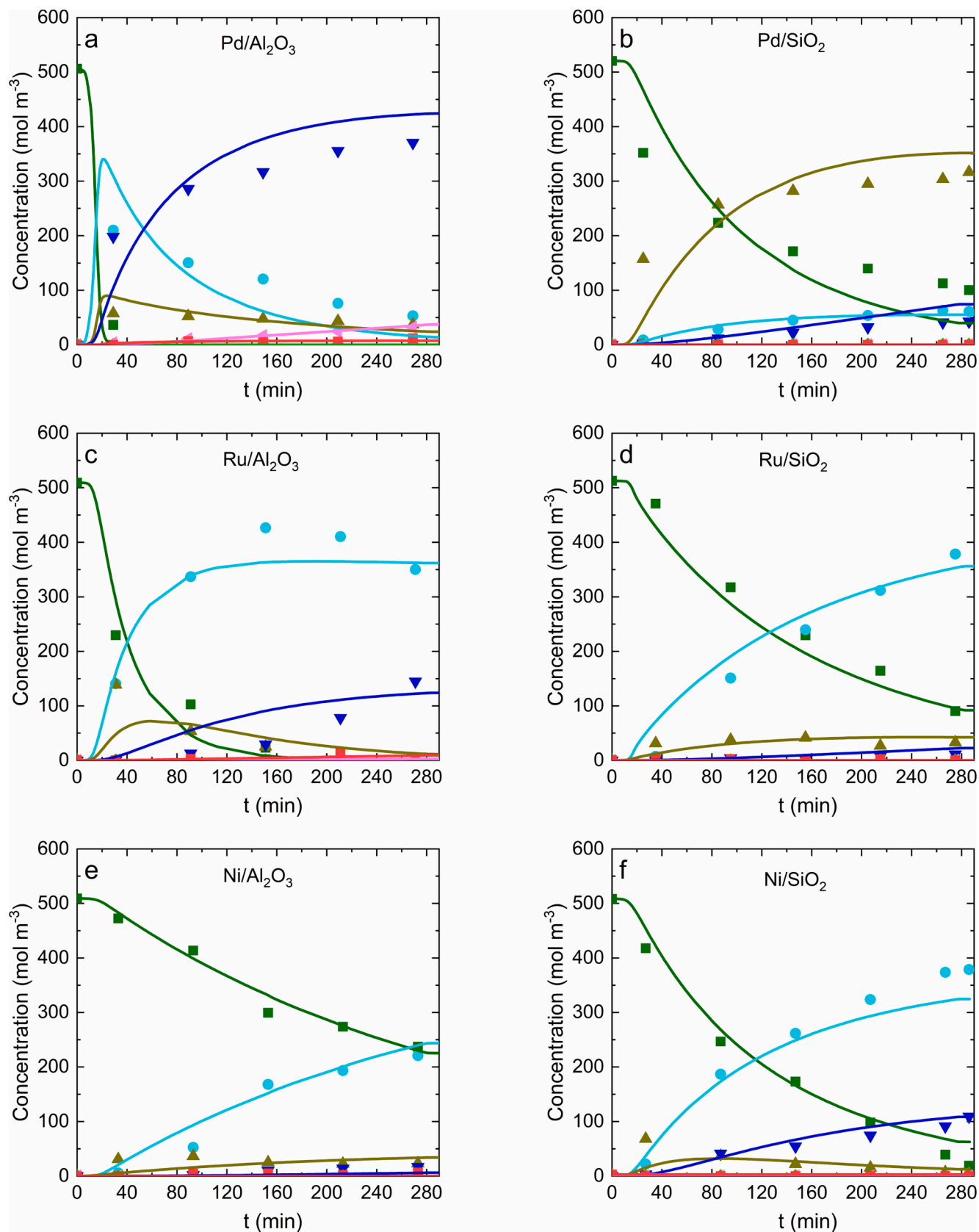
Fig. 7. Kinetic screening at 200 °C. 60 bar of pure hydrogen, 0.2 wt% of catalyst and 5 wt% of furfural mixed in tetrahydrofuran were used. FUR, FA, THFUR, THFA, MF, MTHF, OR.

Table 5

Kinetic parameters of surface reactions occurring on active metal sites, obtained by regression analysis.

i	Pd/Al$_2$O$_3$	Pd/SiO$_2$	Ru/Al$_2$O$_3$	Ru/SiO$_2$	Ni/Al$_2$O$_3$	Ni/SiO$_2$
Reaction rate constants (k_i^M) at 175 °C [s^{-1}]						
1	$2.67 \bullet 10^4$	$3.59 \bullet 10^3$	$7.52 \bullet 10^3$	$7.80 \bullet 10^2$	$7.40 \bullet 10^2$	$3.41 \bullet 10^3$
2	$6.01 \bullet 10^3$	$3.77 \bullet 10^4$	$2.25 \bullet 10^3$	$2.42 \bullet 10^2$	$4.46 \bullet 10^2$	$1.39 \bullet 10^3$
3	$1.94 \bullet 10^3$	$1.95 \bullet 10^3$	$7.07 \bullet 10^3$	$2.44 \bullet 10^2$	$1.26 \bullet 10^3$	$9.90 \bullet 10^3$
4	$6.05 \bullet 10^3$	$7.31 \bullet 10^{-1}$	$1.07 \bullet 10^{-2}$	$7.35 \bullet 10^{-3}$	0	0
5	0	0	0	0	0	0
6	$1.80 \bullet 10^2$	0	7.74	0	0	0
7	0	0	0	0	0	0
8	$1.72 \bullet 10^1$	0	7.54	0	0	0
Activation energy ($E_{a,i}$) [kJ mol^{-1}]						
1	$3.7 \bullet 10^{-3}$	29.6	47.6	54.8	106.6	53.8
2	15.3	$7.3 \bullet 10^{-7}$	68.6	22.4	$1.1 \bullet 10^{-3}$	28.9
3	19.4	19.4	5.3	84.7	6.0	57.1
4	$8.9 \bullet 10^{-4}$	58.2	576.0	213.5	n.a.	n.a.
5	n.a.	n.a.	n.a.	n.a.	n.a.	n.a.
6	9.9	n.a.	173.9	n.a.	n.a.	n.a.
7	n.a.	n.a.	n.a.	n.a.	n.a.	n.a.
8	120.9	n.a.	160.3	n.a.	n.a.	n.a.

Table 7

Maximum TOF values obtained on metallic sites during the tests at 150 °C and 200 °C.

i	Pd/Al$_2$O$_3$	Pd/SiO$_2$	Ru/Al$_2$O$_3$	Ru/SiO$_2$	Ni/Al$_2$O$_3$	Ni/SiO$_2$
TOF$_i$ at 150 °C [s^{-1}]						
1	$1.4 \bullet 10^1$	$3.9 \bullet 10^{-1}$	4.7	$5.0 \bullet 10^{-1}$	$2.3 \bullet 10^{-1}$	2.2
2	2.3	6.4	$9.9 \bullet 10^{-1}$	$2.5 \bullet 10^{-1}$	$6.8 \bullet 10^{-1}$	1.3
3	$1.6 \bullet 10^{-1}$	$3.3 \bullet 10^{-1}$	$4.4 \bullet 10^{-1}$	$9.4 \bullet 10^{-1}$	$1.1 \bullet 10^{-1}$	$5.1 \bullet 10^{-1}$
4	3.1	$4.4 \bullet 10^{-6}$	$2.9 \bullet 10^{-8}$	$8.2 \bullet 10^{-8}$	0	0
5	0	0	0	0	0	0
6	$9.2 \bullet 10^{-1}$	0	$1.4 \bullet 10^{-4}$	0	0	0
7	0	0	0	0	0	0
8	$1.3 \bullet 10^{-3}$	0	$1.2 \bullet 10^{-3}$	0	0	0
Total*	$1.8 \bullet 10^1$	7.0	5.8	$7.5E \bullet 10^{-1}$	$9.5 \bullet 10^{-1}$	3.5
TOF$_i$ at 200 °C [s^{-1}]						
1	$2.4 \bullet 10^1$	5.0	$1.9 \bullet 10^1$	5.1	6.6	$1.3 \bullet 10^1$
2	7.3	$3.5 \bullet 10^1$	7.1	$7.9 \bullet 10^{-1}$	8.6	3.7
3	$6.2 \bullet 10^{-1}$	2.3	1.9	$1.3 \bullet 10^{-1}$	$1.4 \bullet 10^{-1}$	2.0
4	4.6	$2.6 \bullet 10^{-4}$	$4.8 \bullet 10^{-2}$	$2.2 \bullet 10^{-4}$	0	0
5	0	0	0	0	0	0
6	$1.5 \bullet 10^{-1}$	0	$3.4 \bullet 10^{-2}$	0	0	0
7	0	0	0	0	0	0
8	$2.7 \bullet 10^{-1}$	0	$7.9 \bullet 10^{-2}$	0	0	0
Total*	$3.5 \bullet 10^1$	$4.1 \bullet 10^1$	$2.7 \bullet 10^1$	5.9	7.5	$1.8 \bullet 10^1$

* Highest obtained cumulative TOF during the reaction.

kinetics on metallic sites), while only affecting ring opening reactions at higher temperatures. The addition of Al$_2$O$_3$ support also clearly suggests synergistic effect on Pd activity, compared to the monometallic Pd/C catalyst (Table 6).

Pd/SiO$_2$ showed a high ring hydrogenation activity, while the aldehyde group hydrogenation was partially inhibited·THFUR was observed as the main product (70 % yield at 200 °C) at all tested temperatures with no decarbonylation or OR products observed. The maximum cumulative TOF per mass of catalyst (Table 6) was generally lower compared to Pd/Al$_2$O$_3$ due to a lower concentration of active sites (Table 3), which can also be clearly seen from the slower FUR conversion (Figs. 5 – 7 and Table S2). However, the maximum cumulative TOF per active site was comparable and even higher at 200 °C (Table 6– 7). Pd/SiO$_2$ still offered higher activity and selectivity towards furfural ring hydrogenation at all tested temperatures and showed a similar or slightly better total activity compared to monometallic Pd/C (Table 6).

The Ru/Al$_2$O$_3$ catalyst was active mostly for the aldehyde group

Table 6

Highest cumulative TOF values obtained during the reaction at 200 °C. Pd, Ru and Ni with 5 % metal content, deposited on carbon, Al$_2$O$_3$ and SiO$_2$ supports are compared.

	Pd	Ru	Ni
Overall rate [s^{-1}]			
C^a	$7.6 \bullet 10^{-2}$	$3.7 \bullet 10^{-2}$	$6.9 \bullet 10^{-2}$
Al$_2$O$_3$	$3.5 \bullet 10^1$	$2.7 \bullet 10^1$	7.5
SiO$_2$	$4.1 \bullet 10^1$	5.9	$1.8 \bullet 10^1$
Total TOF [mol g^{-1} s^{-1}]^b			
C^a	$3.4 \bullet 10^{-5}$	$1.1 \bullet 10^{-4}$	$3.8 \bullet 10^{-5}$
Al$_2$O$_3$	$3.3 \bullet 10^{-4}$	$1.3 \bullet 10^{-4}$	$1.5 \bullet 10^{-5}$
SiO$_2$	$4.7 \bullet 10^{-5}$	$5.0 \bullet 10^{-5}$	$4.0 \bullet 10^{-5}$

^{a} Values taken from Ref. [36].
^{b} Recalculated by multiplying TOF [s^{-1}] with the concentration of active sites (C$_{AS}$), to obtain TOF, defined per mass of catalyst.

hydrogenation (75 % FA yield at 175 °C) and less for ring hydrogenation. The ring opening reactions were observed to a lower degree. A similar TOF (per catalyst mass) was achieved compared to the monometallic Ru/C (Table 6), suggesting that Al$_2$O$_3$ support did not meaningfully change the total activity of Ru, although the activity of individual surface sites (TOF per active site) was found to be much higher. However, sequential decarbonylation and ring opening reactions were greatly inhibited.

The Ru/SiO$_2$ catalyst was found to exhibit mostly aldehyde group hydrogenation with some ring hydrogenation. Although a similar reaction pathway was found with Ru/Al$_2$O$_3$, all elementary reactions were generally slower (Table 7). The total activity TOF (per active site) was also mostly lower compared to the other tested catalysts, which could be a result of inhibitory interactions between SiO$_2$ and Ru. However, by comparing the TOF (defined per mass of catalyst) values at 200 °C (Table 6), its activity was still higher in comparison to Pd/C, Pd/SiO$_2$ and all Ni based (Ni/C, Ni/Al$_2$O$_3$, Ni/SiO$_2$) catalysts, which is attributed to a greater amount of active sites (higher specific surface).

The Ni/Al$_2$O$_3$ catalyst showed a poor activity (48 % FA yield at 200 °C), especially at lower temperatures. As it was found out in our previous work [36], the monometallic Ni selectively catalyses only the reactions of the aldehyde group (hydrogenation, followed by decarbonylation). The aldehyde group hydrogenation also occurred when using Al$_2$O$_3$ as the support. Some ring hydrogenation and no decarbonylation were observed. The TOF (per mass of catalyst) was the lowest compared to all tested catalysts including the carbon-supported ones (Table 6). The strong interaction between Ni and Al$_2$O$_3$, coupled with the partially unreduced NiO could explain the weak performance of Ni/

Al_2O_3 in comparison to other catalysts, according to the results from H_2–TPR (Fig. S3) [55].

Lastly, Ru/SiO_2 showed a better activity compared to Ni/Al_2O_3, and a similar selectivity. Aldehyde group hydrogenation preferentially occurred on the Ni surface, with ring hydrogenation was more notable. Although FA was still the main product (63.9 % yield at 200 °C) at all tested temperatures, a noticeable amount of THFA was observed at higher temperatures. Ru/SiO_2 catalyst has shown a slightly lower activity (TOF, defined per mass of catalyst) compared to monometallic Ni (Table 6), while the choice of SiO_2 as support inhibited decarbonylation.

This work provides attempting to quantitatively describe the interplay of metallic and acidic sites and their interphase to the activity and selectivity of furfural hydrodeoxygenation reactions. Methodology applied is relatively simple, based on several simplifications and relatively superficial materials characterisation inputs. Further works should involve more detailed characterisation to provide clearer insight in the catalyst structure, especially the interphase of metallic and acidic sites. Also, a systematic study involving a high-throughput syntheses of materials is required to increase the number of samples to validate the conclusions or to propose new mechanisms and quantitative descriptors.

4. Conclusion

Six different combinations of catalytically active metals and supports (Pd/Al_2O_3, Pd/SiO_2, Ru/Al_2O_3, Ru/SiO_2, Ni/Al_2O_3, Ni/SiO_2) were synthetized and thoroughly characterized, then their performance for furfural hydrotreatment were evaluated at 150 °C, 175 °C and 200 °C. CO-TPD and NH_3-TPD were utilized to determine the amount of metallic and acidic sites, respectively, as well as to estimate adsorption and desorption parameters by fitting the experimental data. The adsorption properties of the metallic sites clearly changed between the different supports (Al_2O_3 or SiO_2), while the adsorption on acidic (support) sites remained largely unchanged.

The micro-kinetic model formulated to characterize surface reactions at active metal sites demonstrated its efficacy in accurately portraying kinetics across various tested catalysts. Notably, the model dismissed the catalytic inactivity of acidic support sites when considered in isolation. Nevertheless, their consequential interaction with adjacent metallic sites and the formation of the interphase emerged as a crucial factor. The kinetic activity and selectivity of the reactions on each individual active metal (Pd, Ru, Ni) sites varied depending on the used support likely as a result of bimetallic interactions. Catalyst activity was found to correlate with catalyst textural properties and interphase probabilities, which correlate with the number of interphase sites. Generally, the Al_2O_3 supported catalysts had larger interphase probabilities compared to the SiO_2 supported ones. The activity of Al_2O_3 supported catalysts increased with the interphase probabilities, while activity decreased for the SiO_2 supported catalysts.

Generally, the decarbonylation and ring opening reactions were inhibited when using either Al_2O_3 or SiO_2 as support. Ring hydrogenation was found to proceed on all catalysts, as noticeable amounts of THFUR (and in most cases THFA) formed on all the tested catalysts. However, Ru and Ni based catalysts still showed poor ring hydrogenation activity. Based on these results, it remains unclear if the support had any effect on ring hydrogenation over Pd metallic sites. The aldehyde group activity was most affected by the choice of different supports. Al_2O_3 was found to have a synergistic effect on the Pd activity, a minor effect on the Ru activity and an inhibitory effect on the Ni activity. SiO_2 generally inhibited aldehyde group hydrogenation and ring opening reactions.

CRediT authorship contribution statement

Rok Šivec: Data curation, Investigation, Software, Writing – original draft. **Brett Pomeroy:** Investigation, Validation, Writing – review & editing. **Matej Huš:** Conceptualization, Investigation, Methodology, Software, Supervision, Writing – original draft, Writing – review & editing. **Blaž Likozar:** Funding acquisition, Resources. **Miha Grilc:** Conceptualization, Methodology, Project administration, Resources, Software, Supervision, Writing – original draft, Writing – review & editing.

Declaration of competing interest

The authors declare that they have no known competing financial interests or personal relationships that could have appeared to influence the work reported in this paper.

Data availability

Data will be made available on request.

Acknowledgements

Appendix A. Supplementary data

Supplementary data to this article can be found online at https://doi.org/10.1016/j.cej.2024.149284.

References

[1] M.S. Singhvi, D.V. Gokhale, Lignocellulosic biomass: Hurdles and challenges in its valorization, Appl. Microbiol. Biotechnol. 103 (2019) 9305–9320, https://doi.org/10.1007/S00253-019-10212-7/FIGURES/3.

[2] X. Li, P. Jia, T. Wang, Furfural: A Promising Platform Compound for Sustainable Production of C_4 and C_5 Chemicals, ACS Catal. 6 (2016) 7621–7640, https://doi.org/10.1021/acscatal.6b01838.

[3] T. Werpy, G. Petersen, Top Value Added Chemicals from Biomass: Volume I-Results of Screening for Potential Candidates from Sugars and Synthesis Gas, U.S, Dep. Energy (2004), https://doi.org/10.2172/15008859.

[4] J.J. Bozell, G.R. Petersen, Technology development for the production of biobased products from biorefinery carbohydrates—the US Department of Energy's "Top 10" revisited, Green Chem. 12 (2010) 539–554, https://doi.org/10.1039/b922014c.

[5] K. Dussan, B. Girisuta, D. Haverty, J.J. Leahy, M.H.B. Hayes, Kinetics of levulinic acid and furfural production from Miscanthus×giganteus, Bioresour. Technol. 149 (2013) 216–224, https://doi.org/10.1016/j.biortech.2013.09.006.

[6] D.M. Alonso, J.Q. Bond, J.A. Dumesic, Catalytic conversion of biomass to biofuels, Green Chem. 12 (2010) 1493, https://doi.org/10.1039/c004654j.

[7] M. Dashtban, A. Gilbert, P. Fetehi, Production of Furfural: Overview and Challenges, J. Sci. Technol. for. Prod. Process. 2 (2012) 44–53.

[8] L.T. Mika, E. Cséfalvay, Á. Németh, Catalytic Conversion of Carbohydrates to Initial Platform Chemicals: Chemistry and Sustainability, Chem. Rev. 118 (2018) 505–613, https://doi.org/10.1021/acs.chemrev.7b00395.

[9] J.N. Chheda, G.W. Huber, J.A. Dumesic, Liquid-Phase Catalytic Processing of Biomass-Derived Oxygenated Hydrocarbons to Fuels and Chemicals, Angew. Chem., Int. Ed. 46 (2007) 7164–7183, https://doi.org/10.1002/anie.200604274.

[10] M. Besson, P. Gallezot, C. Pinel, Conversion of Biomass into Chemicals over Metal Catalysts, Chem. Rev. 114 (2014) 1827–1870, https://doi.org/10.1021/cr4002269.

[11] M.J. Climent, A. Corma, S. Iborra, Conversion of biomass platform molecules into fuel additives and liquid hydrocarbon fuels, Green Chem. 16 (2014) 516–547, https://doi.org/10.1039/c3gc41492b.

[12] R. Mariscal, P. Maireles-Torres, M. Ojeda, I. Sádaba, M. López Granados, Furfural: a renewable and versatile platform molecule for the synthesis of chemicals and fuels, Energy Environ. Sci. 9 (2016) 1144–1189, https://doi.org/10.1039/c5ee02666k.

[13] G. Machado, S. Leon, F. Santos, R. Lourega, J. Dullius, M.E. Mollmann, P. Eichler, Literature Review on Furfural Production from Lignocellulosic Biomass, Nat. Resour. 07 (2016) 115–129, https://doi.org/10.4236/nr.2016.73012.

[14] A.E. Eseyin, P.H. Steele, An overview of the applications of furfural and its derivatives, Int. J. Adv. Chem. 3 (2015) 42, https://doi.org/10.14419/ijac.v3i2.5048.

[15] S. Chen, R. Wojcieszak, F. Dumeignil, E. Marceau, S. Royer, How Catalysts and Experimental Conditions Determine the Selective Hydroconversion of Furfural and 5-Hydroxymethylfurfural, Chem. Rev. 118 (2018) 11023–11117, https://doi.org/10.1021/acs.chemrev.8b00134.

[16] Y. Wang, D. Zhao, D. Rodríguez-Padrón, C. Len, Recent Advances in Catalytic Hydrogenation of Furfural, Catalysts. 9 (2019) 796, https://doi.org/10.3390/catal9100796.

[17] K. Gupta, R.K. Rai, S.K. Singh, Metal Catalysts for the Efficient Transformation of Biomass-derived HMF and Furfural to Value Added Chemicals, ChemCatChem. 10 (2018) 2326–2349, https://doi.org/10.1002/cctc.201701754.

[18] R. Šivec, B. Likozar, M. Grilc, Surface kinetics and transport phenomena modelling for furfural hydrotreatment over Pd/C in isopropanol and tetrahydrofuran, Appl. Surf. Sci. 541 (2021) 148485, https://doi.org/10.1016/j.apsusc.2020.148485.

[19] S. Bhogeswararao, D. Srinivas, Catalytic conversion of furfural to industrial chemicals over supported Pt and Pd catalysts, J. Catal. 327 (2015) 65–77, https://doi.org/10.1016/j.jcat.2015.04.018.

[20] Y. Nakagawa, K. Takada, M. Tamura, K. Tomishige, Total Hydrogenation of Furfural and 5-Hydroxymethylfurfural over Supported Pd–Ir Alloy Catalyst, ACS Catal. 4 (2014) 2718–2726, https://doi.org/10.1021/cs500620b.

[21] S. Sitthisa, D.E. Resasco, Hydrodeoxygenation of Furfural Over Supported Metal Catalysts: A Comparative Study of Cu, Pd and Ni, Catal. Lett. 141 (2011) 784–791, https://doi.org/10.1007/s10562-011-0581-7.

[22] N.S. Biradar, A.A. Hengne, S.N. Birajdar, R. Swami, C.V. Rode, Tailoring the product distribution with batch and continuous process options in catalytic hydrogenation of furfural, Org. Process Res. Dev. 18 (2014) 1434–1442, https://doi.org/10.1021/OP500196X.

[23] C. Li, G. Xu, X. Liu, Y. Zhang, Y. Fu, Hydrogenation of Biomass-Derived Furfural to Tetrahydrofurfural Alcohol over Hydroxyapatite-Supported Pd Catalyst under Mild Conditions, Ind. Eng. Chem. Res. 56 (2017) 8843–8849, https://doi.org/10.1021/acs.iecr.7b02046.

[24] S.M. Rogers, C.R.A. Catlow, C.E. Chan-Thaw, A. Chutia, N. Jian, R.E. Palmer, M. Perdjon, A. Thetford, N. Dimitratos, A. Villa, P.P. Wells, Tandem Site- and Size-Controlled Pd Nanoparticles for the Directed Hydrogenation of Furfural, ACS Catal. 7 (2017) 2266–2274, https://doi.org/10.1021/acscatal.6b03190.

[25] B. Chen, F. Li, Z. Huang, G. Yuan, Tuning catalytic selectivity of liquid-phase hydrogenation of furfural via synergistic effects of supported bimetallic catalysts, Appl. Catal., a. 500 (2015) 23–29, https://doi.org/10.1016/j.apcata.2015.05.006.

[26] N.S. Biradar, A.M. Hengne, S.N. Birajdar, P.S. Niphadkar, P.N. Joshi, C.V. Rode, Single-pot formation of THFAL via catalytic hydrogenation of FFR over Pd/MFI catalyst, ACS Sustain. Chem. Eng. 2 (2014) 272–281, https://doi.org/10.1021/sc400302b.

[27] L.J. Liu, H.M. Guo, B. Xue, H. Lou, M. Chen, Hydrogenation in supercritical conditions catalyzed by palladium supported on modified activated carbon, RSC Adv. 5 (2015) 66704–66710, https://doi.org/10.1039/c5ra14284a.

[28] R. Albilali, M. Douthwaite, Q. He, S.H. Taylor, The selective hydrogenation of furfural over supported palladium nanoparticle catalysts prepared by sol-immobilisation: Effect of catalyst support and reaction conditions, Catal, Sci. Technol. 8 (2018) 252–267, https://doi.org/10.1039/c7cy02110k.

[29] S.H. Pang, C.A. Schoenbaum, D.K. Schwartz, J.W. Medlin, J. Will Medlin, Effects of Thiol Modifiers on the Kinetics of Furfural Hydrogenation over Pd Catalysts, ACS Catal. 4 (2014) 3123–3131, https://doi.org/10.1021/cs500598y.

[30] Y. Nakagawa, K. Tomishige, Total hydrogenation of furan derivatives over silica-supported Ni-Pd alloy catalyst, Catal. Commun. 12 (2010) 154–156, https://doi.org/10.1016/j.catcom.2010.09.003.

[31] R. Huang, Q. Cui, Q. Yuan, H. Wu, Y. Guan, P. Wu, Total Hydrogenation of Furfural over Pd/Al2O3 and Ru/ZrO2 Mixture under Mild Conditions: Essential Role of Tetrahydrofurfural as an Intermediate and Support Effect, ACS Sustain. Chem. Eng. 6 (2018) 6957–6964, https://doi.org/10.1021/acssuschemeng.8b00801.

[32] R.M. Mironenko, O.B. Belskaya, T.I. Gulyaeva, A.I. Nizovskii, A.V. Kalinkin, V. I. Bukhtiyarov, A.V. Lavrenov, V.A. Likholobov, Effect of the nature of carbon support on the formation of active sites in Pd/C and Ru/C catalysts for hydrogenation of furfural, Catal. Today. 249 (2015) 145–152, https://doi.org/10.1016/j.cattod.2014.10.037.

[33] J.J. Musci, A.B. Merlo, M.L. Casella, Aqueous phase hydrogenation of furfural using carbon-supported Ru and RuSn catalysts, Catal. Today. 296 (2017) 43–50, https://doi.org/10.1016/j.cattod.2017.04.063.

[34] L.J. Durndell, G. Zou, W. Shangguan, A.F. Lee, K. Wilson, Structure-Reactivity Relations in Ruthenium Catalysed Furfural Hydrogenation, ChemCatChem. 11 (2019) 3927–3932, https://doi.org/10.1002/cctc.201900481.

[35] P. Panagiotopoulou, D.G. Vlachos, Liquid phase catalytic transfer hydrogenation of furfural over a Ru/C catalyst, Appl. Catal., a. 480 (2014) 17–24, https://doi.org/10.1016/j.apcata.2014.04.018.

[36] R. Šivec, M. Huš, B. Likozar, M. Grilc, Furfural hydrogenation over Cu, Ni, Pd, Pt, Re, Rh and Ru catalysts: Ab initio modelling of adsorption, desorption and reaction micro-kinetics, Appl. Catal., b. 436 (2022), https://doi.org/10.1016/J.CEJ.2022.135070.

[37] S.H. Pang, N.E. Love, J.W. Medlin, Synergistic effects of alloying and thiolate modification in furfural hydrogenation over Cu-based catalysts, J. Phys. Chem. Lett. 5 (2014) 4110–4114, https://doi.org/10.1021/jz502153q.

[38] Y. Song, W. Li, M. Zhang, T. Keyi, Hydrogenation of furfuryl alcohol to tetrahydrofurfuryl alcohol on NiB/SiO2 amorphous alloy catalyst, Front. Chem. Eng. China. 1 (2007) 151–154, https://doi.org/10.1007/s11705-007-0028-2.

[39] Y. Wang, P. Prinsen, K.S. Triantafyllidis, S.A. Karakoulia, P.N. Trikalitis, A. Yepez, C. Len, R. Luque, ⊥ A. Yepez, C. Len, R. Luque, Comparative Study of Supported Monometallic Catalysts in the Liquid-Phase Hydrogenation of Furfural: Batch Versus Continuous Flow, ACS Sustain. Chem. Eng. 6 (2018) 9831–9844, https://doi.org/10.1021/acssuschemeng.8b00984.

[40] Y. Nakagawa, H. Nakazawa, H. Watanabe, K. Tomishige, Total Hydrogenation of Furfural over a Silica-Supported Nickel Catalyst Prepared by the Reduction of a Nickel Nitrate Precursor, ChemCatChem. 4 (2012) 1791–1797, https://doi.org/10.1002/cctc.201200218.

[41] M. Manikandan, A.K. Venugopal, K. Prabu, R.K. Jha, R. Thirumalaiswamy, Role of surface synergistic effect on the performance of Ni-based hydrotalcite catalyst for highly efficient hydrogenation of furfural, J. Mol. Catal. A Chem. 417 (2016) 153–162, https://doi.org/10.1016/j.molcata.2016.03.019.

[42] T.V. Kotbagi, H.R. Gurav, A.S. Nagpure, S.V. Chilukuri, M.G. Bakker, Highly efficient nitrogen-doped hierarchically porous carbon supported Ni nanoparticles for the selective hydrogenation of furfural to furfuryl alcohol, RSC Adv. 6 (2016) 67662–67668, https://doi.org/10.1039/c6ra14078e.

[43] M.Y. Chen, C.B. Chen, B. Zada, Y. Fu, Perovskite type oxide-supported Ni catalysts for the production of 2,5-dimethylfuran from biomass-derived 5-hydroxymethylfurfural, Green Chem. 18 (2016) 3858–3866, https://doi.org/10.1039/c6gc00432f.

[44] L. Liu, H. Lou, M. Chen, Selective hydrogenation of furfural to tetrahydrofurfuryl alcohol over Ni/CNTs and bimetallic Cu[sbnd]Ni/CNTs catalysts, Int. J. Hydrogen Energy. 41 (2016) 14721–14731, https://doi.org/10.1016/j.ijhydene.2016.05.188.

[45] J. Wu, G. Gao, J. Li, P. Sun, X. Long, F. Li, Efficient and versatile CuNi alloy nanocatalysts for the highly selective hydrogenation of furfural, Appl. Catal., B. 203 (2017) 227–236, https://doi.org/10.1016/j.apcatb.2016.10.038.

[46] Y. Nakagawa, M. Tamura, K. Tomishige, Supported Metal Catalysts for Total Hydrogenation of Furfural and 5-Hydroxymethylfurfural, J. Japan Pet. Inst. 60 (2017) 1–9, https://doi.org/10.1627/JPI.60.1.

[47] S. Sang, Y. Wang, W. Zhu, G. Xiao, Selective hydrogenation of furfuryl alcohol to tetrahydrofurfuryl alcohol over Ni/γ-Al2O3 catalysts, Res. Chem. Intermed. 43 (2017) 1179–1195, https://doi.org/10.1007/S11164-016-2691-8/FIGURES/9.

[48] Z. Zhang, K. Sun, Y. Ma, Q. Liu, Q. Li, S. Zhang, Y. Wang, Q. Liu, D. Dong, X. Hu, Nanofibers and amorphous Ni/Al2O3 catalysts — effect of steric hindrance on hydrogenation performance, Catal, Sci. Technol. 9 (2019) 4510–4514, https://doi.org/10.1039/C9CY00985J.

[49] K. Yan, C. Jarvis, T. Lafleur, Y. Qiao, X. Xie, Novel synthesis of Pd nanoparticles for hydrogenation of biomass-derived platform chemicals showing enhanced catalytic performance, RSC Adv. 3 (2013) 25865–25871, https://doi.org/10.1039/C3RA43619E.

[50] Y. Zhao, Facile synthesis of Pd nanoparticles on SiO2 for hydrogenation of biomass-derived furfural, Environ. Chem. Lett. 12 (2014) 185–190, https://doi.org/10.1007/S10311-013-0424-4/TABLES/1.

[51] R. López-Asensio, J.A. Cecilia, C.P. Jiménez-Gómez, R. García-Sancho, R. Moreno-Tost, P. Maireles-Torres, Selective production of furfuryl alcohol from furfural by catalytic transfer hydrogenation over commercial aluminas, Appl. Catal., a. 556 (2018) 1–9, https://doi.org/10.1016/J.APCATA.2018.02.022.

[52] S. Dekkar, S. Tezkratt, D. Sellam, K. Ikkour, K. Parkhomenko, A. Martinez-Martin, A.C. Roger, Dry Reforming of Methane over Ni–Al2O3 and Ni–SiO2 Catalysts: Role of Preparation Methods, Catal. Lett. 1508 (150) (2020) 2180–2199, https://doi.org/10.1007/S10562-020-03120-3.

[53] J.S. Kwon, J.S. Kim, H.S. Lee, M.S. Lee, Surface Modification of SiO2 for Highly Dispersed Pd/SiO2 Catalyst, J. Nanosci. Nanotechnol. 19 (2018) 882–887, https://doi.org/10.1166/JNN.2019.15943.

[54] F. Ruimei, C. Yajuan, S. Zhonghua, G. Maochu, C. Yaoqiang, Catalytic Activity of C3H8 over Fresh and Aged Pd/Al2O3 Close-Coupled Catalysts, Rare Met, Mater. Eng. 46 (2017) 1231–1236, https://doi.org/10.1016/S1875-5372(17)30142-X.

[55] Y. Xu, X.H. Du, J. Li, P. Wang, J. Zhu, F.J. Ge, J. Zhou, M. Song, W.Y. Zhu, A comparison of Al2O3 and SiO2 supported Ni-based catalysts in their performance for the dry reforming of methane, J. Fuel Chem. Technol. 47 (2019) 199–208, https://doi.org/10.1016/S1872-5813(19)30010-6.